Published OnlineFirst March 15, 2019; DOI: 10.1158/0008-5472.CAN-18-2015

Molecular Cell Biology

Cancer Research

AQP4 Aggregation State Is a Determinant for Glioma Cell Fate

Laura Simone[1], Francesco Pisani[2], Maria G. Mola[2], Manuela De Bellis[2], Giuseppe Merla[3], Lucia Micale[3], Antonio Frigeri[4,5], Angelo L. Vescovi[1], Maria Svelto[2,6,7], and Grazia P. Nicchia[2,5]

Abstract

The glial water channel protein aquaporin-4 (AQP4) forms heterotetramers in the plasma membrane made of the M23-AQP4 and M1-AQP4 isoforms. The isoform ratio controls AQP4 aggregation into supramolecular structures called orthogonal arrays of particles (AQP4-OAP). The role of AQP4 aggregation into OAP in malignant gliomas is still unclear. In this study, we demonstrate that AQP4 aggregation/disaggregation into OAP influences the biology of glioma cells. Selective expression of the OAP-forming isoform M23-AQP4 (AQP4-OAP) triggered cell shape changes in glioma cells associated with alterations to the F-actin cytoskeleton that affected apoptosis. By contrast, expression of M1-AQP4 (AQP4-tetramers), which is unable to aggregate into OAP, ameliorated glioma cell invasiveness, improved cell migration, and increased methalloproteinase-9 activity. Two prolines (254 and 296) at the C-terminus tail were shown to be important in mediating the relationship between the actin cytoskeleton and AQP4-OAP and AQP4-tetramers. In conclusion, this study demonstrates that AQP4 aggregation state might be an important determinant in orienting glioma cells to persist or perish. AQP4 disaggregation may potentiate invasiveness potential, whereas AQP4 aggregation may activate the apoptotic path. This study shows a new perspective on the role of AQP4 in brain tumors not necessarily associated with edema formation but with AQP4 aggregation/disaggregation dynamics and their link with the actin cytoskeleton.

Significance: This study demonstrates how AQP4 aggregation influences plasma membrane dynamics to alter cell proliferation, invasiveness, migration, and apoptotic potential in glioma cells.

Introduction

Aquaporin-4 (AQP4) is the central nervous system (CNS) water channel protein highly expressed at astrocyte foot processes, forming specialized microdomains at the interfaces between blood (blood–brain barrier) and cerebrospinal fluid (CSF; CSF–brain barrier; ref. 1). AQP4 is expressed as two major isoforms called M1-AQP4 and M23-AQP4 forming heterotetramers, which in turn spontaneously aggregate into square well-ordered structures called orthogonal arrays of particles (OAP; ref. 2). When the shorter M23-AQP4 is expressed alone, very large OAPs are formed. If the longer M1-AQP4 isoform is expressed alone, no OAPs or very small OAPs are visible. Simultaneous cotransfection of the two isoforms leads to OAPs of different sizes, depending on the ratio of M23-AQP4 and M1-AQP4 isoforms (3). The higher the ratio is, the larger in size are the OAPs and *vice versa*. AQP4-tetramers, formed by M1-AQP4, are mobile in the plasma membrane and therefore able to rapidly diffuse toward the lamellipodium to sustain faster cell migration (4). In contrast, the very low mobile AQP4-OAPs sustain the opposite function of cell adhesion, therefore being important for AQP4-polarized expression at glial endfoot microdomains where they support AQP4 interaction with the extracellular matrix (5) and actin cytoskeleton (6–9). M1-AQP4 and M23-AQP4 are always coexpressed in native tissues and having opposite functions allows astrocytes to regulate OAP size, depending on their needs (migration or cell adhesion/polarization), without altering global brain water permeability (4).

Alteration of brain fluid homeostasis is a common feature of brain tumors. There is extensive literature on the role of aquaporins in tumor biology, including tumor-associated edema, tumor cell migration, tumor proliferation, and tumor angiogenesis, indicating the need for AQP inhibitors as potentially useful anticancer drugs (10–12). The role for endothelial aquaporin-1 (AQP1) in the context of tumor angiogenesis is well-described (13, 14). It is associated with AQP1-dependent endothelial cell migration. In contrast, unveiling the role of AQP4 in brain tumors seems to be more complex.

Several authors have shown a very strong AQP4 upregulation in brain tumors compared with healthy tissue. Interestingly, AQP4

[1]Fondazione IRCCS Casa Sollievo della Sofferenza, Cancer Stem Cells Unit, San Giovanni Rotondo, Italy. [2]Department of Bioscience, Biotechnology and Biopharmaceutics and Centre of Excellence in Comparative Genomics, University of Bari Aldo Moro, Bari, Italy. [3]Division of Medical Genetics, Fondazione IRCCS Casa Sollievo della Sofferenza Hospital, San Giovanni Rotondo, Italy. [4]School of Medicine, Department of Basic Medical Sciences, Neuroscience and Sense Organs, University of Bari Aldo Moro, Bari, Italy. [5]Department of Neuroscience, Albert Einstein College of Medicine, Yeshiva University, New York, Bronx, New York. [6]Institute of Biomembranes and Bioenergetics, National Research Council, Bari, Italy. [7]National Institute of Biostructures and Biosystems (INBB), Rome, Italy.

Note: Supplementary data for this article are available at Cancer Research Online (http://cancerres.aacrjournals.org/).

Corresponding Author: Grazia P. Nicchia, University of Bari Aldo Moro, Via Orabona, 4, 70125 Bari, Italy. Phone: 39-080-5443335; Fax: 39-080-5443388; E-mail: graziapaola.nicchia@uniba.it

doi: 10.1158/0008-5472.CAN-18-2015

Published OnlineFirst March 15, 2019; DOI: 10.1158/0008-5472.CAN-18-2015

upregulation is associated with altered AQP4-OAP localization in human glioma samples (15) with compromised AQP4-polarized expression at the perivascular endfeet (16, 17). An interesting study by Noell and colleagues reports none or only small OAPs on glioblastoma samples analyzed by freeze-fracture electron microscopy, indicating that redistribution of AQP4 and OAPs could be one of the earliest indicators of glioma transformation (17). Interestingly, although a correlation between the decrease in OAPs and increasing grade of malignancy of astrocytomas has been reported, this was not consistent with an upregulation of M1-AQP4 in relation to M23-AQP4 (18).

The different functions reported for AQP4 in astrocyte physiology, depending on the size of AQP4-OAPs (19), and the strong reduction of OAPs in human glioma samples despite a massive increase in AQP4 expression (16, 17), allowed us to hypothesize that the state of AQP4 aggregation into OAPs could influence the biology of glial cells. Therefore, in the present study, cell phenotypes implicated in tumor cell biology, such as cell morphology and cytoskeleton organization, invasiveness, and apoptosis, were analyzed after transfection of cells with M23-AQP4 (forming AQP4-OAPs) or with M1-AQP4 (forming AQP4-tetramers). The study has been conducted on the two cell lines most used as experimental models of glioma, the U87 MG and the U251 MG having several differences in terms of phenotype and biological properties (20, 21). HeLa cells have been considered here as a control cell line of a tumor not of CNS origin.

The results show that although AQP4-tetramers potentiate glioma cell invasiveness, AQP4-OAPs favor the apoptotic path, therefore indicating that AQP4 aggregation state might be an important key as to whether glioma cells persist or perish.

Materials and Methods

Ethic statements

The studies were conducted in accordance with the ethical standards of the institutional and/or national research committee and with the 1964 Helsinki declaration and its later amendments or comparable ethical standards. The animal use protocol for this study has been approved by the Italian Ministry of Health (Approved Project n. 710/2017-PR) in compliance with the European directive on animal use for research and Italian law on animal care. The GL95 culture was derived from a patient affected by a IV grade glioma after obtaining written-informed consent under IRCCS Casa Sollievo della Sofferenza review board approval (Project n. 11268).

Animals

AQP4 KO pups with a CD1 genetic background (22) and age-matched controls were used for astrocyte primary cultures prepared as described below. The mice were bred in the approved facility at the University of Bari. Mice were kept under a 12-hour dark to light cycle, at constant room temperature and humidity ($22°C \pm 2°C$, 75%), with food and water *ad libitum*, and supplied with environmental enrichment materials, such as toys and shelters.

Astrocyte primary cultures

Mouse astrocyte primary cultures were prepared from newborn pups and validation was performed by GFAP staining, as previously described (23). Cells were cultured in DMEM-Glutamax medium supplemented with 10% FBS, 100 U mL^{-1} penicillin, and 100 mg mL^{-1} streptomycin, and maintained at 37°C in a 5% CO_2 incubator. All the cell culture products were purchased from Thermoscientific (www.thermofisher.com). Cells were used at passage 1 or 2, and *Mycoplasma* testing was conducted by nuclear staining with DAPI.

Glioma primary cultures

Cells from a glioblastoma obtained from surgery were mechanically dissociated into single cells using sterile scalpels. Tumor short-term cells suspension was cultured in a poly-lysine–coated T25flask at 37°C and 5% CO_2 and expanded in DMEM/F12 medium containing 10% FCS and 1% penicillin/streptomycin. All the cell culture products were purchased from Thermoscientific (www.thermofisher.com). Cells were used from passages 10 to 13. *Mycoplasma* testing was conducted with MycoAlert Substrate (https://bioscience.lonza.com).

Cell lines and transfection

The following cell lines were acquired, and their identity was authenticated from the ATCC (www.lgcstandards-atcc.org): U87 MG (ATCC HTB-14) cell line, derived from a malignant glioma from a female patient by explant technique (24), the C6 (ATCC CCL-107) cell line, established from a rat glial tumor induced by *N*-nitrosomethylurea (25), the DI-TNC1 (ATCC CRL-2005) cell line, established from primary cultures of type 1 astrocytes from brain diencephalon tissue of 1-day-old rats (26), the B16F10 (ATCC CRL-6475) cell line, established from tumoral melanoma skin of mouse (27), and the HeLa (ATCC CCL-2) cell line, derived from human cervical carcinoma (28). The U251 MG (ICLC HTL99014) cell line, derived from human glioblastoma astrocytoma (29), was acquired from cell bank IRCSS AOU San Martino IST (www.iclc.it) and authenticated by short tandem repeat profile. Cells were used from passages 174 to 185.

Mycoplasma testing was routinely conducted with MycoAlert Substrate (https://bioscience.lonza.com) or by fluorescence staining with DAPI. The cells were maintained at 37°C in a 5% CO_2 incubator. Cell culture reagents were purchased from Euroclone (www.euroclonegroup.it).

Twenty-four hours before transfection, the cells at 70% confluence were plated using antibiotic-free medium. Transient transfection was carried out using Lipofectamine 2000 (Invitrogen, www.thermofisher.com) in OptiMEM growth medium according to the manufacturer's protocol and analyzed after 36 hours.

Antibodies

The following primary antibodies were used: goat polyclonal anti-AQP4 (C-19) (sc-9888), rabbit polyclonal anti-AQP4 (H-80) (sc-20812), and goat polyclonal anti-actin (I-19) (sc-1616).

Phalloidin Alexa Fluor 488–conjugated (A12379; www.thermofisher.com) was used to stain F-Actin.

The secondary antibodies used for immunofluorescence analysis were donkey anti-goat Alexa Fluor 594–conjugated (A11058), donkey anti-goat Alexa Fluor 488–conjugated (A11055), and donkey anti-rabbit Alexa Fluor 488–conjugated (A21207).

The following secondary antibodies were used for Western blot: donkey anti-goat IgG-HRP (sc-2020) and goat anti-rabbit IgG-HRP (sc-2004; https://www.scbt.com/scbt/home;jsessionid=geZqCYpPrb283ItDHGPGoA7yiWfNaM9FOwh_Kp4CtHAre2rCAvOr!805379577).

Published OnlineFirst March 15, 2019; DOI: 10.1158/0008-5472.CAN-18-2015

Constructs and site-specific mutagenesis

Human and rat M1-AQP4 and M23-AQP4 coding sequences were cloned into pTarget (www.Promega.com) and pmCherry-N1 (www.Clontech.com) vectors. The previously characterized mutated form of M1-AQP4 (M23I), demonstrated to give rise exclusively to AQP4-tetramers (30), was used. All the M23-AQP4 mutants, containing the mutations described in Supplementary Table S1, were obtained by site-specific mutagenesis (QuikChange II Site–Directed Mutagenesis Kit; www.Agilent.com) according to the manual instructions. Briefly, the human M23-AQP4 was cloned into pTarget vector and used as a template in a long high fidelity PCR performed with PfuUltra high fidelity DNA polymerase (www.Promega.com). The site-specific mutant primers were designed using the web-based QuikChange primer design program from Stratagene available online. All constructs were fully sequenced (www.Agilent.com).

The CellLight ER-RFP (www.thermofisher.com) fusion construct of endoplasmic reticulum (ER) signal sequence of calreticulin and KDEL (ER retention signal) TagRFP was used to specifically target ER.

Immunofluorescence and quantitative analysis

Cells were fixed in 4% paraformaldehyde for 15 minutes, washed 3 times in PBS, and permeabilized with 0.3% Triton X-100. After blocking using 0.1% gelatine for 30 minutes at room temperature, cells were incubated for 1 hour with primary antibodies and washed with PBS gelatin. Cells were finally incubated with Alexa Fluor–conjugated secondary antibodies and mounted with a medium containing 50% glycerol, 1% n-propylgallate in PBS, and DAPI for nuclear staining. Immunostained cells were observed with a photomicroscope equipped for epifluorescence and 16x, 40x oil PL FL FLUOTAR objectives (www.leica-microsystems.com). Digital images were obtained with a DMX1200 camera (Nikon) and processed using LAS AF software (Leica Microsystems GmbH). Once captured, the auto contrast function was applied to the whole images using Photoshop CS5 (www.adobe.com).

Quantitative analysis after immunofluorescence was conducted on 3 to 5 different fields from each of 3 independent experiments (as indicated in each figure legend) performed on 3 different days. All the cells in each field were properly counted, depending on the assay, using Imagej or Fiji software (https://imagej.nih.gov/ij/), and analyzed using GraphPad Prism 6 (www.graphpad.com/scientific-software/prism).

Morphologic analysis

Morphological analysis was performed by evaluating the presence of a shrunk morphology (retraction of cytoplasm and plasma membrane) with a star-like phenotype and a number of branches greater than four. The cells considered as positive for change in morphology were very clearly distinguishable in each field from the other cells. The analysis was performed in a blind manner by two independent investigators. The number of cells with altered morphology was counted using Image J or Fiji software (https://imagej.nih.gov/ij/) and analyzed using GraphPad Prism 6 (www.graphpad.com/scientific-software/prism).

ER-density analysis

To measure the local density of ER, AQP4 and ER-RFP cotransfected cells were analyzed by quantitative immunofluorescence analysis. Briefly, AQP4-positive cells were identified, and at least four different rectangular regions of interest (ROI; fixed squared 40 μm^2) per cell were selected (31). The mean of the fluorescence of ER-RFP for each ROI was collected using LASX software and processed by Prism6 software for statistics analysis.

Confocal microscopy

Confocal images were obtained with an automated inverted Leica TCS SP8 confocal microscope using a 63 and 100x HC PL Apo oil CS2 objective. All confocal images were collected using 594 laser line for excitation and a pinhole diameter of 1 Airy unit. The optical series covered at least 15 optical slices, from the bottom to the top of the cells, with a raster size of 1024 × 1024 in the x–y planes and a z-step of 0.5 μm between optical slices. Three-dimensional (3D) images and projections from z-stack were constructed and processed using Leica Application Suite X software (www.leicamicrosystems.com). Cell volume was calculated with imageJ using the plug-in Volumest, a semi-automated program used to measure the total volume of the threshold fluorescently labeled cells obtained as a cumulative z-stack. Briefly, an area value for a single section was calculated and the plug-in then generated a 3D volume calculated from the entire stack.

Western blotting and quantitative analysis

Cells grown in 24 multiwell formats were washed once in ice-cold PBS and dissolved in 100 μL of RIPA lysis buffer (10 mmol/L Tris-HCl, pH 7.4, 140 mmol/L NaCl, 1% Triton X-100, 1% Na deoxycholate, 0.1% SDS, 1 mmol/L Na_3VO_4, 1 mmol/L NaF, and 1 mmol/L EDTA) added with a cocktail of protease inhibitors (http://www.merckmillipore.com). Lysis was performed on ice for 30 minutes, and the samples were then centrifuged at 17,000 × g for 30 minutes. The protein content of the supernatant was measured with a bicinchoninic acid (BCA) Protein Assay Kit (www.thermofisher.com). Equal amounts of cell lysates (10 μg total protein/lane) were dissolved in Laemmli Sample Buffer (www.bio-rad.com) with added 50 mmol/L dithiothreitol, heated to 37°C for 10 minutes, loaded and separated by SDS-PAGE on a 13% polyacrylamide, and transferred to polyvinylidene difluoride membranes (http://www.merckmillipore.com). Membranes with blotted proteins were incubated with primary antibodies, washed, and incubated with peroxidase-conjugated secondary antibodies (22). Reactive proteins were revealed with an enhanced chemiluminescent detection system (www.thermofisher.com), visualized on a Versadoc imaging system (www.bio-rad.com), and analyzed by GraphPad Prism 6 (www.graphpad.com/scientific-software/prism).

For quantitative analysis, three independent Western blots were performed in different days from cells at independent passages. The bands revealed, indicated for each experiment, were quantified by densitometry analysis using ImageJ software. The optical density value was determined for equal-sized boxes drawn around antibody-stained bands (https://imagej.nih.gov/ij/) and analyzed using GraphPad Prism 6 (www.graphpad.com/scientific-software/prism).

Ratios of G- to F-actin

Ratios of G- to F-actin were determined using the G-Actin/F-actin In Vivo Assay Kit (BK037; http://www.cytoskeleton.com), as previously described (32). Briefly, 5 × 10^5 cells were scraped,

Published OnlineFirst March 15, 2019; DOI: 10.1158/0008-5472.CAN-18-2015

resuspended in Lysis and F-actin Stabilization Buffer, and centrifuged at 350 × *g* for 5 minutes. Note that 100 µL of the supernatants was ultracentrifuged at 100,000 × *g* for 1 hour to separate F-actin from soluble G-actin. The pellets were resuspended in a volume equal to that of the supernatant, and equal volumes of supernatant and pellet samples were analyzed by Western blotting with actin and AQP4 antibodies. The revealed bands were quantified as described above.

Apoptosis and necrosis quantification

Apoptosis and necrosis were determined using the Apoptosis and Necrosis Quantification Kit (30017; www.biotium.com). Briefly, cells were washed twice with PBS, incubated with FITC–Annexin V and EthD-III, and analyzed by epifluorescence microscopy. WT U87 MG cells following administration of H_2O_2 2 mmol/L for 6 hours at 37°C and staurosporine 5 µM for 4 hours were used as positive controls of necrosis and apoptosis, respectively.

Primary amino acid sequence multiple alignment analysis

The multiple alignment analysis of AQP4 primary amino acid sequences was performed using Clustal Omega (www.ebi.ac.uk/Tools/msa/clustalo/). All the sequences were obtained from NCBI, Entrez Gene Reference Sequences.

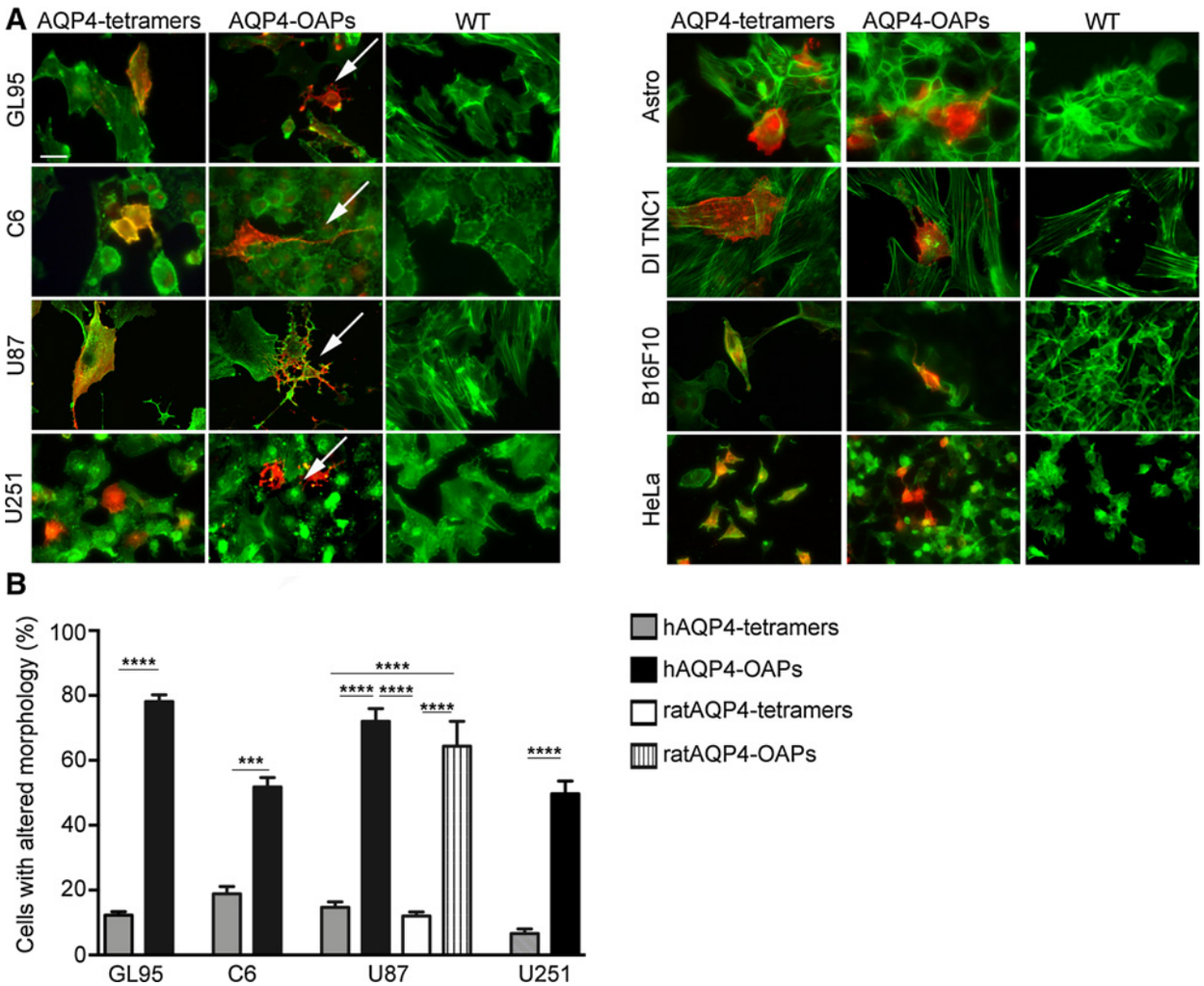

Figure 1.

Effects of AQP4-tetramer and AQP4-OAP expression on morphology and cytoskeleton of tumor and nontumor cell lines. **A,** Epifluorescence images of cells transfected with M1-AQP4 isoform (AQP4-tetramers) and M23-AQP4 isoform (AQP4-OAPs) and relative WT (WT). AQP4 staining is shown in red, and F-actin cytoskeleton is visualized with phalloidin (green). Left, GL95 (human glioma primary culture); C6 (rat glioma-immortalized cell line); U87 (human glioma-immortalized cell line); U251 (human glioma-immortalized cell line). Right, Astro (astrocyte primary cultures prepared from AQP4 KO mice); DI TNC1 (rat-immortalized astrocyte cell line); B16F10 (murine melanoma cell line); HeLa (adenocarcinoma-immortalized cell line). Arrows, change in cell shape in AQP4-OAP–transfected cells. Scale bar, 50 µm. **B,** Histobar showing the percentage of cells with altered morphology calculated for GL95, C6, U87, and U251 cells transfected with human AQP4-tetramers (hAQP4-tetramers) and AQP4-OAPs (hAQP4-OAPs). U87 were also analyzed after transfection with the rat sequence of AQP4-tetramers (ratAQP4-tetramers) and AQP4-OAPs (ratAQP4-OAPs). Values are expressed as mean ± SEM of percentage of cells with altered cell morphology out of the total number of transfected cells per field. ***, $P < 0.0005$; ****, $P < 0.0001$; $n = 3$.

Published OnlineFirst March 15, 2019; DOI: 10.1158/0008-5472.CAN-18-2015

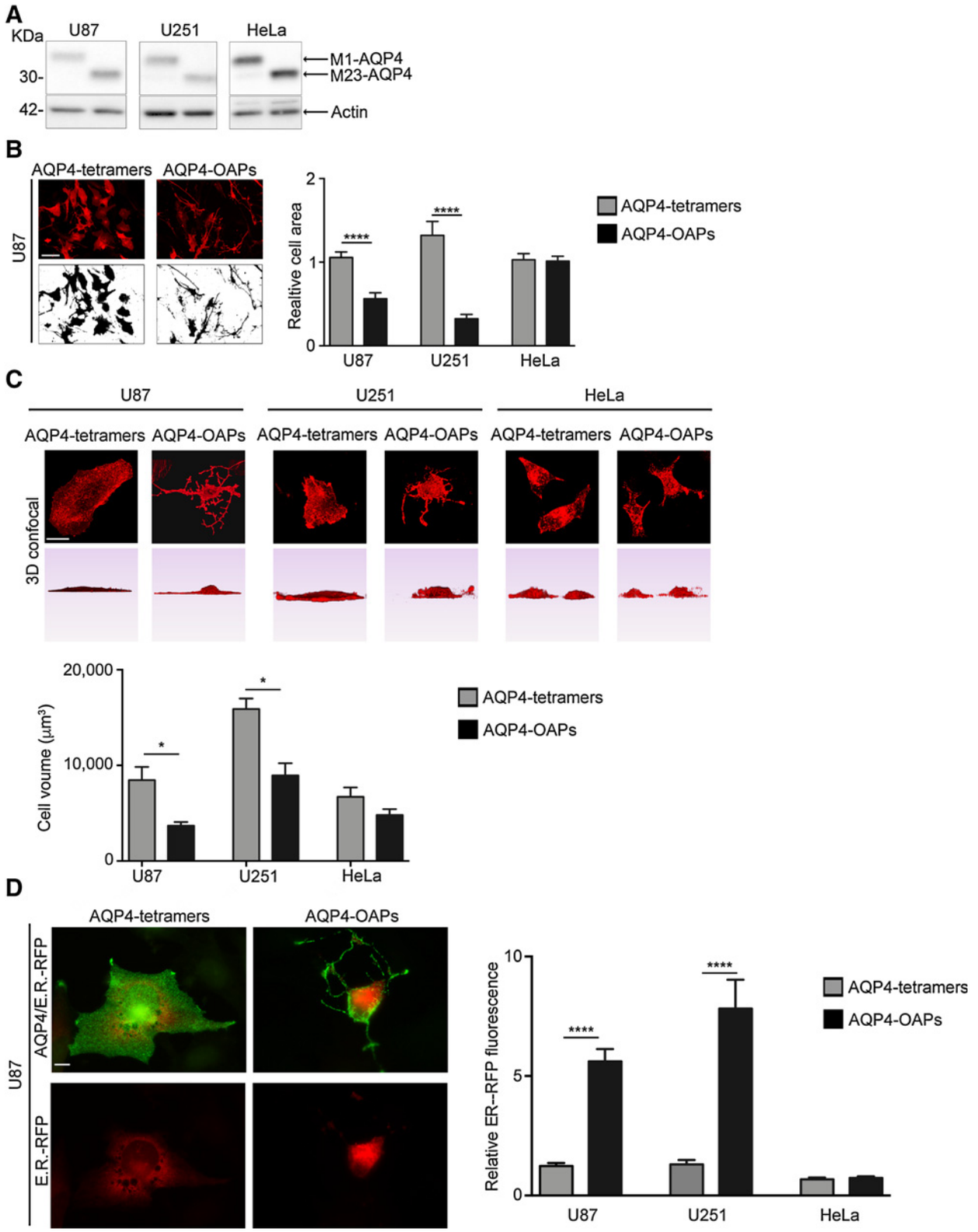

Published OnlineFirst March 15, 2019; DOI: 10.1158/0008-5472.CAN-18-2015

The Swiss-pdb Viewer application was used to visualize C-terminus tail and H-bond involving residues. The initial structure of AQP4 was obtained from the Protein Data Bank (PDB entry 3GD8) with a resolution of 1.8Å obtained by X-ray diffraction (33) and was used to generate the model. The existence of hydrogen bonds was predicted with the compute Hbonds tool of the Swiss-Pdb Viewer (https://spdbv.vital-it.ch/).

In vitro invasion assays

Invasion transwell assays were performed using the Boyden chambers as previously described (34). Briefly, the upper side of the filters was coated with Matrigel 1 mg/mL. Cells (5×10^5) were seeded onto the layer of Matrigel in their growth medium without serum FBS. Twelve hours after plating, unmigrated cells on the upper side of the filters were mechanically removed, whereas those invading onto the 10% FBS contained on the lower side were fixed and counted with Image J software.

Zymography

Gelatin zymography analysis was performed using the conditioned medium collected at the end of the "invasion assay" described in the previous paragraph (35). Briefly, culture media were centrifuged, mixed with a 10% SDS-containing loading buffer, and subjected to SDS-PAGE using a 10% gel containing 1 mg/mL gelatin. At the end of the run, the gels were washed twice with 100 mL distilled water containing 25% Triton and incubated in 100 mL of "Development buffer" (50 mmol/L Tris–HCl, pH 7.4, and 10 mmol/L $CaCl_2$) at 37°C for 42 hours. The gels were then stained with 0.125% Coomassie Blue R250 for 1 hour, and the gelatinolytic activity of MMP9 was detected as clear bands against a blue background. The band corresponding to the total MMP9 was quantified as previously described for ECL-revealed bands.

Statistical analysis

Statistically significant differences were computed using the Student *t* test and two-way ANOVA analysis, the level being set at $P < 0.05$. All statistical analyses were performed using GraphPad Prism version 6.00 (www.graphpad.com/scientific-software/prism). Data are expressed as mean ± SEM.

Results

AQP4-OAP expression triggers cell shape changes in glioma cells

To assess whether AQP4 aggregation into OAPs plays a role in cell morphology and cytoskeletal dynamics under physiologic and/or pathophysiologic conditions, a total of 2 primary cell cultures and 6 different cell lines were analyzed after transfection with the two major human AQP4 isoforms: M1-AQP4 (forming tetramers not able to aggregate into OAPs and later on called "AQP4-tetramers") and M23-AQP4 (forming tetramers able to aggregate into OAPs and later on called "AQP4-OAPs"). In particular, cells of glial-tumor origin (GL95 human primary cultures of glioma, rat C6 glioma cell line, and U87 MG and U251 MG glioblastoma multiforme human cell lines) were compared with healthy astrocytes (AQP4-null mouse astrocyte primary cultures and rat DI TNC1 cell line) and with tumor cells not of CNS origin (B16F10 rat melanoma cell line and the HeLa human cervical adenocarcinoma cell line). Immunofluorescence was used to analyze AQP4 and F-actin expression (Fig. 1A). The results showed that a profound alteration in cell morphology and cytoskeleton was selectively observed in glioma cells when transfected with AQP4-OAPs, whereas no such effect was induced by AQP4-tetramers. In particular, AQP4-OAP expression induced the appearance of cytoskeletal reorganization and cytoplasmic protrusions. Differently, the same cells expressing AQP4-tetramers retained a polygonal shape with mainly an ordered distribution of actin stress fibers. The quantitative analysis (Fig. 1B) revealed the significantly higher frequency of irregular shaped cells in glioma cells expressing human AQP4-OAPs compared with cells transfected with human AQP4-tetramers (GL95: 78.2 ± 2.1% vs. 12.3 ± 2.1%; C6: 48.98 ± 3.82% vs. 18.85 ± 2.25%; U87 MG: 72.02 ± 3.9% vs. 14.72 ± 1.7% for human AQP4 sequences and 64.35 ± 7.68% vs. 12.05 ± 1.25% for rat AQP4 sequences; U251 MG: 49.7 ± 3.9% vs. 6.6 ± 1.4%). No changes were induced either by AQP4-tetramers or AQP4-OAPs in healthy astrocytes and in tumor cells not of CNS origin, indicating that the AQP4-OAP–dependent change of morphology observed is a peculiarity of tumor cells of glial origin, and it is not common with other tumor cells such as melanoma or adenocarcinoma cells and is not common with healthy cells of glial origin like astrocytes.

We selectively focused on human cell lines to detail the effect of AQP4 aggregation in glioma cells. In particular, the two most used cell lines as experimental models of glioma, U87 MG and U251 MG, were studied and compared with the widely used HeLa cells always analyzed in parallel as negative control (Fig. 2). After ascertaining comparable expression levels of M1-AQP4 and M23-AQP4 for each cell line (Fig. 2A), the two-dimensional projected cell area (Fig. 2B) and cell volume (Fig. 2C) were determined by imaging analysis. U87 MG and U251 MG–expressing AQP4-tetramers showed a significantly larger projected area (Fig. 2B) and volume (Fig. 2C) than those expressing AQP4-OAPs, whereas no significant difference was found in HeLa cells analyzed in parallel.

In order to discriminate whether the reduced cell area and volume measured for the two glioma cell lines were due to a simple change of cell morphology or to a cell shrinkage, the density of organelles was investigated using quantitative analysis of ER fluorescence intensity (Fig. 2D). Glioma cells (U87 MG and

Figure 2.

Analysis of U87, U251, and HeLa cell shape parameters after transfection with AQP4-tetramers and AQP4-OAPs. **A,** Immunoblot detection of AQP4 expression levels in U87, U251, and HeLa cells transfected with M1-AQP4 (AQP4-tetramers) and M23-AQP4 (AQP4-OAPs). β-Actin was used to normalize for equal loading. **B,** Left, AQP4 immunofluorescence is shown in red for U87 cells transfected with AQP4-tetramers and AQP4-OAPs. The 2D-topographical image of cell area (black) is shown in parallel and was used for quantification analysis (right). Right, histobar showing the quantification analysis of the relative cell area performed for U87, U251, and HeLa cells. Values are expressed as mean ± SEM. ****, $P < 0.0001$; $n = 3$. Scale bar, 50 μm. **C,** Top, 3D reconstruction of a confocal z-stack of AQP4-OAP–transfected and AQP4-tetramer–transfected U87, U251, and HeLa cells stained with anti-AQP4 antibodies (red). Scale bar, 20 μm. Bottom, histobar showing the quantification of cell volume of the cells transfected as indicated. Values are expressed as mean ± SEM. *, $P < 0.05$; $n = 3$. **D,** Left, the CellLight ER-RFP (red) was used to specifically target ER, whereas AQP4 staining of AQP4-tetramers and AQP4-OAPs is shown in green. Right, histobar showing the relative increase in fluorescence intensity in AQP4-OAP–transfected compared with AQP4-tetramer–transfected cells, as indicated. ****, $P < 0.0001$; $n = 3$. Scale bar, 10 μm.

Published OnlineFirst March 15, 2019; DOI: 10.1158/0008-5472.CAN-18-2015

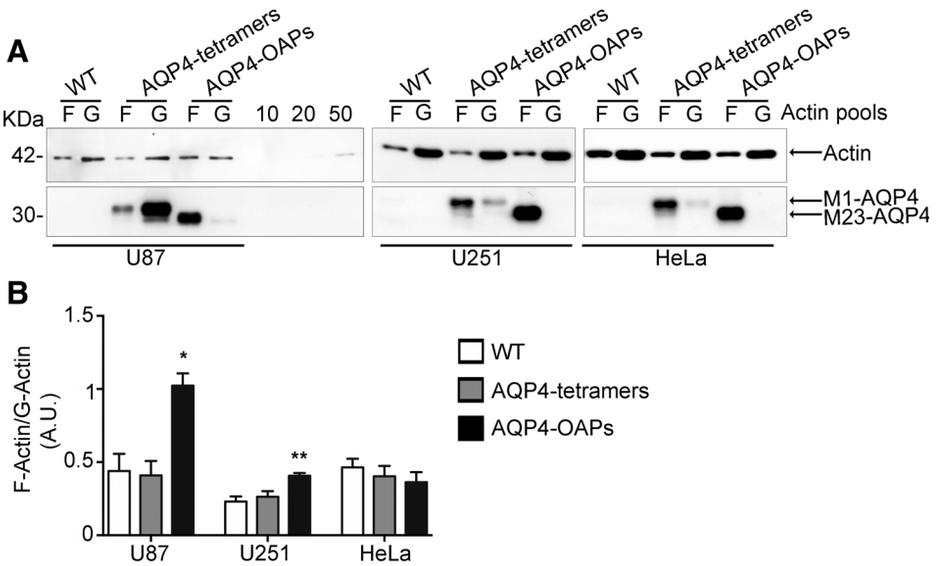

Figure 3.
Effect of AQP4 aggregation into OAPs on F-actin dynamics in U87, U251, and HeLa cells. **A,** Western blot analysis of F-actin (F) and G-actin (G) containing samples in indicated cells, untransfected (WT), and transfected with human M1-AQP4 (AQP4-tetramers) and M23-AQP4 (AQP4-OAPs). Ten ng (10), 20 ng (20), and 50 ng (50) of G-actin standard were loaded as control. **B,** Densitometric analysis of the immunoblot in **A** showing F-actin/G-actin ratio in untransfected (WT), AQP4-tetramer, and AQP4-OAP–transfected U87, U251, and HeLa cells. Values are expressed as mean ± SEM. *, $P < 0.05$; **, $P < 0.001$; $n = 3$.

U251 MG) expressing AQP4-OAPs showed a significant increase in the density of ER compared with the same cells expressing AQP4-tetramers. No differences were found for HeLa cells analyzed in parallel.

These results indicate that AQP4 plasma membrane aggregation into OAPs plays a key role in tumor glial cell morphology and that AQP4 aggregation into OAPs induces cell shrinkage in both glioma cell lines and not in HeLa cells.

AQP4 aggregation into OAPs governs F-actin dynamics in glioma cell and leads to apoptosis

To obtain additional information about AQP4-OAP–induced morphologic and actin organization changes, we performed a quantitative analysis of actin polymerization grade by determining the amount of filamentous actin (F-actin) versus free globular-actin (G-actin), using high-speed centrifugation that allows the G- and F-actin pools to be separated from cell lysates (Fig. 3A). Changes in the relative amount of G-actin and F-actin were investigated in U87 MG, U251 MG, and HeLa cells by Western blot (Fig. 3A). In WT and AQP4-tetramer–transfected glioma cells, the F-actin/G-actin ratio was similarly in favor of G-actin, indicating that the presence of AQP4-tetramers does not significantly affect actin cytoskeleton in either U87 MG or U251 MG. In contrast, transfection of AQP4-OAPs significantly increases the F-actin/G-actin ratio in both U87 MG and U251 MG, although this increase was much higher in U87 MG than in U251 MG (Fig. 3B). These results indicate that AQP4-OAPs significantly affect actin cytoskeleton dynamics in glioma cells with a much more dramatic perturbation for U87 MG in line with their more dramatic change in cell morphology shown in Figs. 1A and 2C. A not statistically significant difference in F-actin/G-actin was found in HeLa cells when transfected with either AQP4-tetramer or AQP4-OAPs compared with WT, indicating that AQP4 expression independently from its aggregation state does not affect cytoskeleton dynamics in HeLa cells. AQP4 immunoblotting performed in parallel on the same fractions (Fig. 3A) revealed interesting results with more similarity between U251 MG and HeLa compared with U87 MG cells. AQP4-OAPs were always selectively present in the F-Actin fraction, indicating that the association between AQP4-OAPs with F-actin is a common feature of the three cell lines analyzed, independently from their origin. In contrast, AQP4-tetramers mainly cosedimented with the F-Actin fraction in U251 MG and HeLa cells even though a small fraction of AQP4-tetramers was always present in the G-actin fraction. The situation appeared to be completely different for U87 MG cells in which the majority of AQP4-tetramers were present in the G-Actin containing fraction and only a small amount in the F-Actin fraction. These results similarly indicate that, in all the cells analyzed, the relationship between AQP4 and actin cytoskeleton depends on the AQP4 aggregation state, with AQP4-OAPs more strongly associated with F-Actin compared with AQP4-tetramers. On the other hand, the specific effect of AQP4-OAPs on glioma cells, shown in Figs. 1 and 2, seems to be associated with an actin perturbation, which is much more pronounced in U87 MG cells and very mild in U251 MG cells. This is in line with the dramatic and milder changes in cell morphology observed for U87 MG and U251 MG cells, respectively.

We later tested whether the shrinking and cytoskeleton changes induced by AQP4-OAPs could be related to the morphologic rearrangements occurring during apoptosis (Fig. 4). In particular, by using Annexin V, U87 MG, U251 MG, and HeLa cells were analyzed for early signs of apoptosis (Fig. 4A). AQP4-OAP–expressing U87 MG and U251 MG showed a relevant staining for Annexin V with a 2-fold increase in the population of apoptotic cells compared with the same cells expressing AQP4-tetramers (Fig. 4B). No differences in Annexin-positive cells were found in HeLa cells between AQP4-tetramer and AQP4-OAP–transfected cells. Figure 4C shows that the morphology was similar between AQP4-OAP expressing U87 MG and WT U87 MG treated with staurosporine to induce apoptosis, whereas no evidence of necrosis was found in AQP4-OAP expressing U87 (Fig. 4C).

AQP4-tetramers increase metastatic potential in glioblastoma multiforme

The contribution of AQP4 aggregation state in tumor cell invasion through the extracellular matrix was tested by using the Boyden chamber assay (Fig. 5). The results show that the invasion ability of AQP4-OAP expressing U87 MG, U251 MG, and HeLa

Published OnlineFirst March 15, 2019; DOI: 10.1158/0008-5472.CAN-18-2015

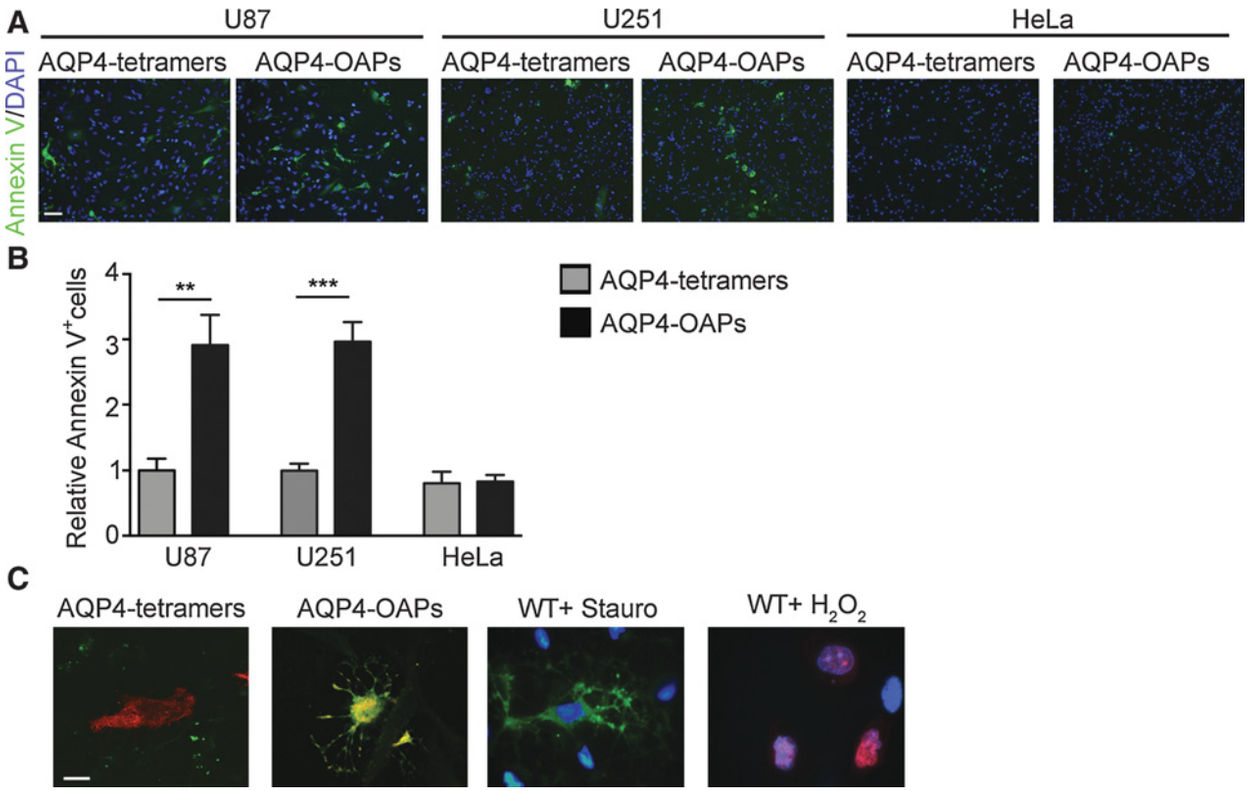

Figure 4.

Effect of AQP4 aggregation into OAPs on apoptosis in U87, U251, and HeLa cells. **A,** Cells, transfected as indicated, stained for Annexin V (green) and DAPI (blue). Scale bar, 50 μm. **B,** Histobar showing the relative increase in Annexin-positive cells counted on experiments shown in **A**. Values are expressed as mean ± SEM of fold increase in Annexin V^+ cells in AQP4-OAP compared with AQP4-tetramer transfected. **, $P < 0.005$; ***, $P < 0.0005$; $n = 3$. **C,** Representative confocal images (merge) of U87 transfected with AQP4-tetramers and AQP4-OAPs stained with AQP4 (red), Annexin V (green), EtD-III (nuclear; red), and DAPI (blue). WT treated with staurosporine (WT + Stauro) and with H_2O_2 (WT + H_2O_2) was used as positive control for apoptosis (green) and necrosis (red), respectively. Scale bar, 20 μm.

cells was not significantly different to the corresponding WT cells. In contrast, AQP4-tetramers significantly increased the ability of both glioma cell lines, U87 MG and U251 MG, to invade the matrix while they did not affect this property in HeLa cells (Fig. 5A and B). These results indicate that controlling the AQP4 aggregation state might be important for glioma cells to acquire higher invasive capability.

To clarify whether the increased capability of AQP4-tetramer–transfected glioma cells was related to a different metalloproteinase activity, zymography experiments were performed to analyze the metalloproteinase-9 (MMP9) activity during the invasion process (36, 37). The results (Fig. 5C and D) revealed that a significantly higher activity of MMP9 could be selectively observed in both glioma cell lines transfected with AQP4-tetramers compared with cells transfected with AQP4-OAPs, whereas no difference in MMP9 activity was revealed between AQP4-tetramer and AQP4-OAP–transfected HeLa cells. These results indicate that the increased invasiveness of AQP4-tetramer expressing glioma cells is sustained by MMP9 activity.

The M23-AQP4 C-terminus is the key in AQP4-OAP–dependent cytoskeleton perturbation

To gain insight into the molecular determinant involved in the cell morphologic and functional changes observed in glioma cells, we first tested a number of mutants of AQP4 in which specific regions in loops A, C, and E were deleted or replaced with the corresponding sequences of AQP0 (Fig. 6A), because AQP0 is also able to aggregate into OAPs the same as AQP4. Most of these mutants (Supplementary Table S1) had previously been used and characterized by our group to identify specific regions of AQP4 extracellular loops involved in the binding with the human autoantibody found in patients affected by Neuromyelitis Optica (38). All the AQP4-OAP mutants correctly targeted the plasma membrane and formed OAPs similar to WT AQP4-OAPs, in terms of number and size, as previously shown (38). This analysis was only performed in U87 MG cell, this being the cell line the most affected by AQP4-OAP transfection in terms of cell morphology and actin cytoskeleton. U87 MG cells transfected with WT and mutated AQP4 isoforms were analyzed for cell morphologic changes by immunofluorescence (Fig. 6B). The quantitative analysis revealed that all the mutants induced the same morphologic changes as AQP4-OAPs, therefore indicating that AQP4-OAP extracellular loops are not involved in the morphologic changes observed in AQP4-OAP–transfected cells. The role of the AQP4 C-terminus was then investigated, as potentially being involved in the morphologic and functional effects observed on U87 and ascribed to AQP4 aggregation into OAPs. To this end, first we

Published OnlineFirst March 15, 2019; DOI: 10.1158/0008-5472.CAN-18-2015

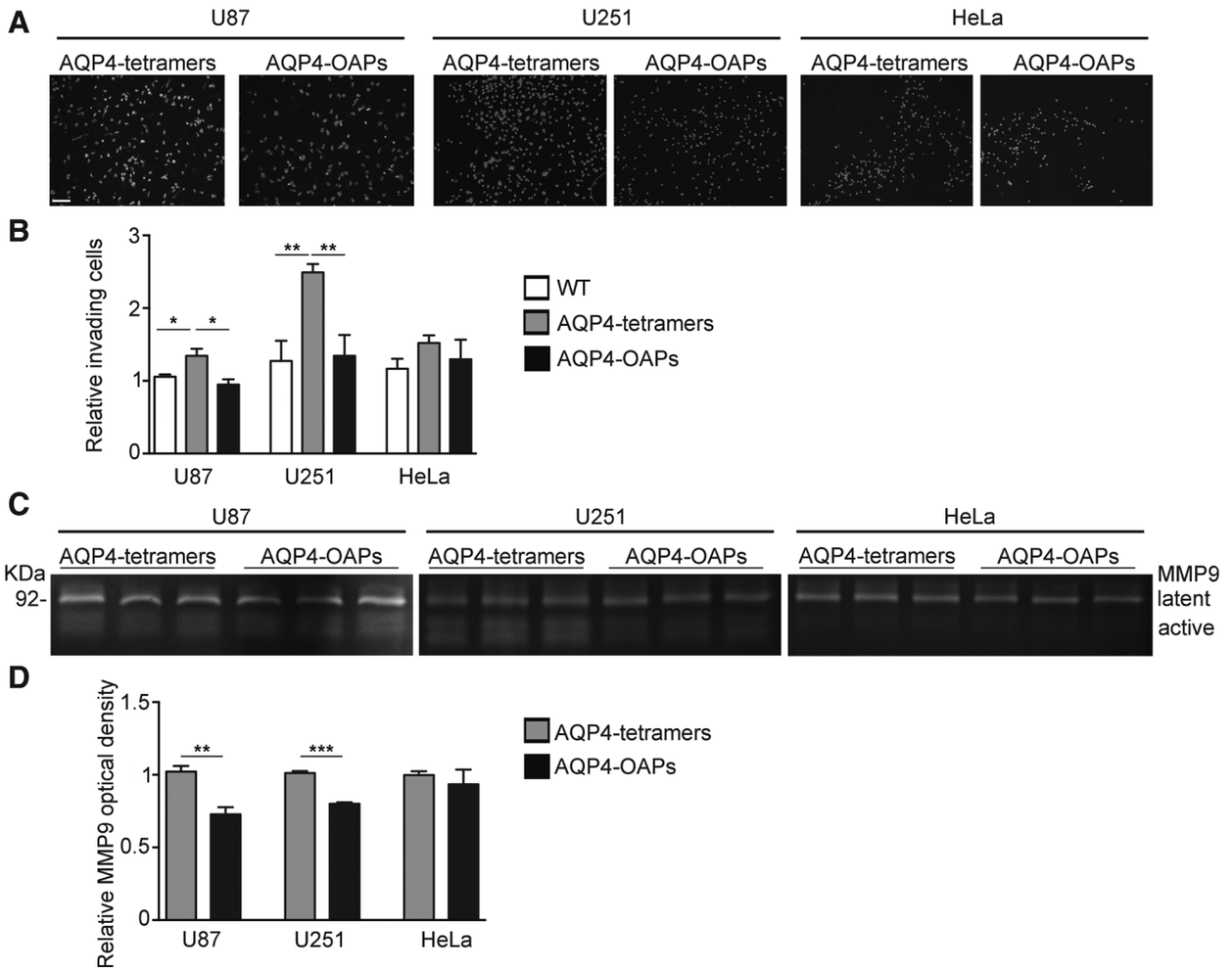

Figure 5.

Effect of AQP4 aggregation into OAPs on invasiveness potential in U87, U251, and HeLa cells. **A,** Representative images of cell invasiveness on Matrigel assay. The three cell lines, transfected as indicated, were subjected to the invasion assay using Boyden chambers for 12 hours. DAPI, blue. Scale bar, 50 μm. **B,** Quantification of the data collected, as described in **A**. The histobar shows the mean ± SEM of invading cells compared with WT cells. *, $P < 0.05$; **, $P < 0.005$; $n = 3$. **C,** Gelatin zymography analysis for MMP9 of conditioned media of U87, U251, and HeLa cells transfected as indicated. **D,** Histobar showing MMP9 activity in AQP4-tetramers transfected compared with AQP4-OAP–transfected cells. **, $P < 0.005$; ***, $P < 0.0005$; $n = 3$.

evaluated the effect of a C-terminus fluorescent tag, such as m-Cherry, by immunofluorescence (Supplementary Fig. S1). Interestingly, M23-AQP4 having a C-terminus mCherry-tail was unable to produce the changes induced by the untagged M23-AQP4 isoform, indicating a key role of this region in the observed modifications in glioma cells.

To evaluate which region of the C-terminus could be directly involved in the observed changes, a multialignment analysis of AQP4 was performed from amphibia to mammals and between mammals of different species (Fig. 7A). Two prolines at positions 254 and 296 and the last six amino acids (PDZ-domain; ref. 47) were highly conserved (Fig. 7A and B) and were the target of the subsequent mutagenesis. The mutagenesis approach was aimed at breaking the predicted β-turn spatial constriction (Fig. 7C). In statistical analyses of residues found in β-turns (39), protein structures display preferences for Pro or Gly at certain β-turn positions. The $i+1$ residue of type II turns is usually Pro. Pro is often found in turns, presumably due to its unique restricted angle, which is entropically favorable at certain turn positions. Glycine is also often found at other positions of different β-turn types because its lack of a β-carbon sterically allows a wider range of angles than other amino acids. Therefore, a double-mutant $P^{254}GP^{296}G$ was generated together with a mutant in which the PDZ domain was deleted ($\Delta^{318\text{-}323}$). M23-AQP4 mutants were in this case transfected in both U87 MG and U251 MG cells, and immunofluorescence was used to analyze and quantify cell morphologic changes (Fig. 7D and E). The results showed that both mutants were able to impair the ability of AQP4-OAPs to induce cell morphologic changes in both glioma cells. This suggests that β-turn spatial constriction and C-terminus orientation are necessary for the OAP interaction with the cytoskeleton. These results confirm the role of the AQP4-OAP C-terminus as cell shape determinant and that the orientation of the tail plays a crucial role in this phenomenon, which, in glioma cells, is

Published OnlineFirst March 15, 2019; DOI: 10.1158/0008-5472.CAN-18-2015

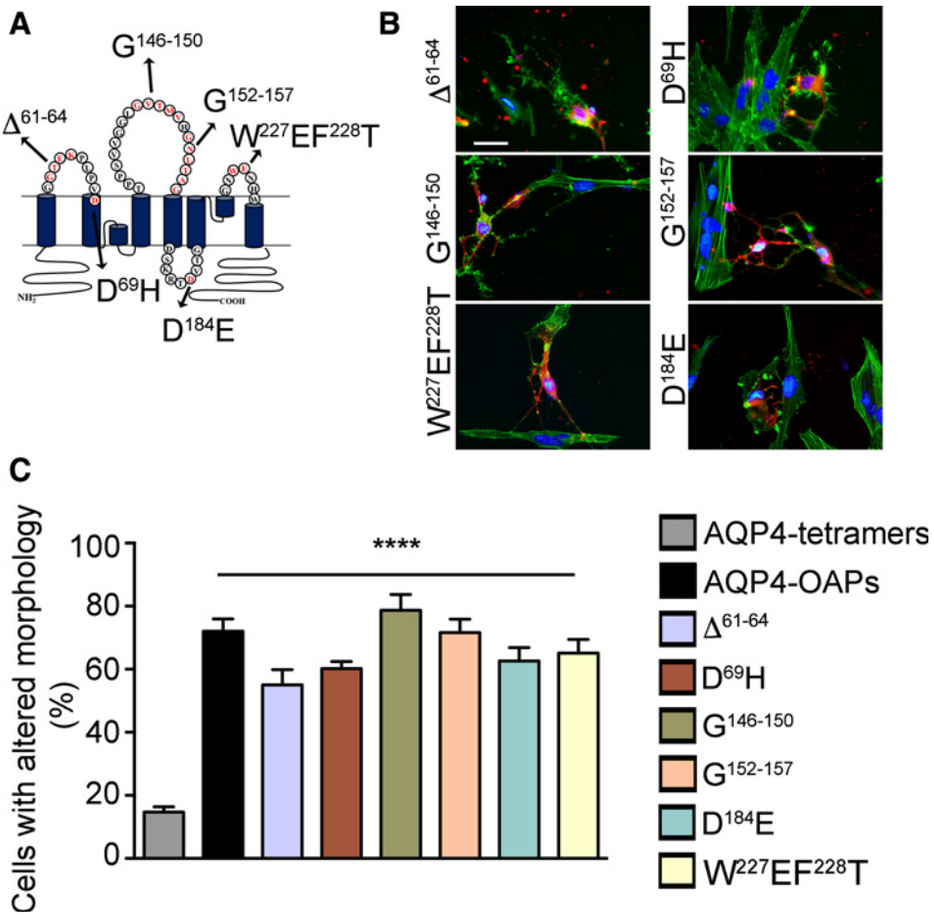

Figure 6.
AQP4 extracellular loop analysis of the amino acids involved in the major changes observed in U87 cell morphology. **A,** Schematic representation of AQP4 amino acid sequence analyzed by mutagenesis (red). For more details, see also Supplementary Table S1. **B,** Representative images of U87 transfected with the mutated OAP-forming isoforms and stained with anti-AQP4 antibody (red) and phalloidin (green) to visualize F-actin. Blue, cell nuclei. Scale bar, 50 μm. **C,** Quantification analysis performed to compare the number of cells with morphologic alteration between U87 cells transfected with AQP4 sequences as indicated. Values are expressed as mean ± SEM of percentage of cells with altered cell morphology on the total number of transfected cells per field. ****, $P < 0.0001$; $n = 3$.

correlated with important functional alterations such as apoptosis and invasiveness.

Discussion

The main novelty of this study is that AQP4 aggregation state is important in glioma cells to determine their fate toward invasiveness or apoptosis and that this control is mediated by a different relationship with the actin cytoskeleton depending on the C-tail of AQP4-OAPs and that of AQP4-tetramers. Although having AQP4-tetramers or AQP4-OAPs does not affect the morphology of normal astrocytes in culture, it makes a significant difference in glioma cells. This study demonstrates that AQP4-OAP expression in glioma cells leads to important cell shrinkage with alteration in actin cytoskeleton and apoptosis. Therefore, the general conclusion is that AQP4 aggregation into OAPs is "deleterious" for glioma cell survival. In contrast, AQP4-tetramer expression increases glioma cell migration, with increased metalloproteinase activity, indicating that AQP4-tetramers are "beneficial" for glioma cells, improving their invasiveness potential. From this perspective, it is not surprising that glioma cell biology is directed toward OAP disassembly into AQP4-tetramers (16, 17, 40), which allows invasiveness to be achieved while avoiding apoptosis.

The "beneficial" role of AQP4-tetramers in glioma cells finds its basis in the functional role amply reported for M1-AQP4 in favoring cell migration both in healthy astrocytes and in glioma cells (41–43). It is interesting to note that the role for M1-AQP4 in cell migration in the context of glioma cell invasiveness is remarkably similar to the role of AQP1 in endothelial cell migration in the context of tumor angiogenesis (44). Notably, AQP1 is only expressed in the tetrameric form.

Differently from AQP4-tetramers, large AQP4-OAPs are not sufficiently mobile in the plasma membrane to address cell migration, being actually involved in sustaining the opposite function of promoting cell adhesion and polarization (4). Neither property is associated with glioma cell biology given that increased cell adhesion would represent an obstacle to glioma cell migration, and polarization is lost in glioma tissue. The "detrimental" role of AQP4-OAPs in glioma cells, shown for the first time in the present study, is based on the observation that M23-AQP4 induces glioma cell apoptosis. If AQP4-tetramers are able to improve the speed of cell migration in both normal astrocytes and glioma cells (4), the induction of apoptosis by AQP4-OAPs is instead specific to glioma cells. In particular, M23-AQP4 expression in glioma cells induces important changes in cell morphology and to the cell cytoskeleton associated with apoptosis. The extent of these changes to cell cytoskeleton and morphology was different in the two cell lines (higher in U87 MG and milder in U251 MG), and this could be related to the higher proliferation, migration, and invasion potential of the U87 compared with the U251 MG cell lines (21, 45).

Published OnlineFirst March 15, 2019; DOI: 10.1158/0008-5472.CAN-18-2015

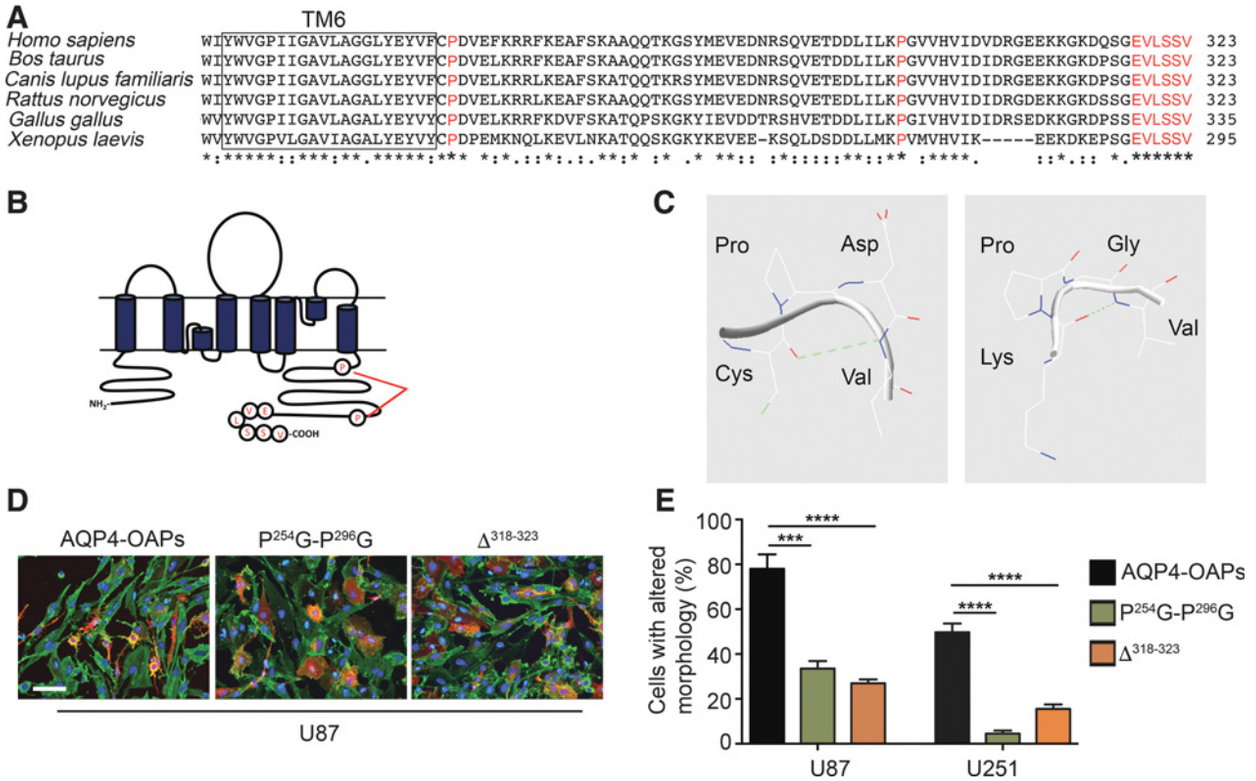

Figure 7.

Mutagenesis analysis on M23-AQP4 C-terminus. **A,** Multialignment analysis of AQP4 C-terminus primary sequence from different species. Pro 254, 296, and the last six amino acids (red bold) are highly conserved. The amino acid positions are referred to M1-AQP4. TM6, transmembrane 6. **B,** Schematic representation of the amino acids analyzed by mutagenesis. **C,** Schematic reconstruction of AQP4 C-terminus tail and predicted β-turn and H-bond (green dashed line) involving P254 and P296 by using spdb viewer software. H-bond forming proline residues and β-turn in AQP4 WT are abolished in double mutants. **D,** Representative images of U87 transfected with the two M23-AQP4 mutants ($P^{254}G$-$P^{296}G$ and $\Delta^{318-323}$) and stained with anti-AQP4 antibodies (red) and phalloidin (green) to visualize F-actin. Both mutations affect AQP4-OAP ability to induce morphologic changes in glioma cells. Scale bar, 100 μm. **E,** Quantification analysis of morphologic alteration induced by M23-AQP4 mutants in experiments performed as described in **D**. The histogram shows the percentage of cells with altered morphology calculated for U87 and U251. Values are expressed as mean ± SEM of percentage of cells with altered cell morphology on the total number of transfected cells per field. ***, $P < 0.0005$; ****, $P < 0.0001$; $n = 3$.

The factors regulating AQP4 expression toward either AQP4-tetramers or AQP4 OAPs remain to be identified. In this context, the membrane curvature-dependent aggregation of AQP4 into OAPs may have interesting implications (46). In particular, the high plasma membrane curvature found at the tip of migrating glioma cells might be sufficient to disaggregate AQP4-OAPs into AQP4-tetramers, therefore facilitating their invasiveness potential.

Cell shrinkage is reported as the first event of the so-called apoptotic volume decrease (AVD) activated by the alteration of ion channel transport mechanisms, mainly leading to K^+ and Cl^- efflux, driving water out of the cell and therefore leading to cell shrinkage (47). A role for water channel proteins in facilitating AVD, by boosting water efflux, has been already proposed by other authors (47). Interestingly, if cell shrinkage in glioma cells is considered the first event in AVD leading to cell death, it is also described as being an important morphologic modification that glioma cells undergo to transform and improve their invasiveness capability. In fact, glioma cells have to face the complex architecture of the brain parenchyma, which represents an obstacle to their dissemination. Secretion of metalloproteinases by glioma cells is important to break the extracellular matrix; meanwhile, reducing their volume helps them to sneak into the brain interstitial space and to migrate following a water flux l generated by AQP4 (11). Glioma cell shrinkage able to increase cell migration (48) is similarly triggered by an ion extrusion in turn driving water efflux, as in AVD. Remarkably, the role of AQP4-mediated water efflux, able to promote both AVD and cell migration, would also be very similar to the corroborated role reported for AQP4 in the RVD occurring in healthy astrocytes exposed to hypotonic conditions. In particular, AQP4 facilitates both the water influx under hypotonic challenge, and the water efflux necessary to bring back the cell volume to its original level (23).

In trying to understand the patho-physiology of glioma cells, based on the different impacts of AQP4-tetramers and AQP4-OAPs on glioma cell fate, the question that arises is whether the general increase in AQP4 expression levels, reported in gliomas, is useful for accelerating migration or for inducing apoptosis, given that both are triggered by AQP4-mediated water efflux. It cannot be related to a different rate of water efflux through M23-AQP4 promoting apoptosis or through M1-AQP4 promoting invasiveness, because it is known that the water permeability is

not different between M1-AQP4 and M23-AQP4 (3). The answer to this question could stand on data in this article, showing that AQP4-tetramers and AQP4-OAPs have a different relationship with the actin cytoskeleton. In the healthy brain, AQP4-OAP interaction with the F-actin cytoskeleton is mediated by the dystrophin-associated protein complex (6, 7), including, in particular, syntrophin, which is directly responsible for AQP4 anchoring in the perivascular pool (49). Interestingly, the endfoot targeting of syntrophin is a key determinant for the OAP size (49). We can therefore speculate that in brain tumors, the remodeling of the actin cytoskeleton associated with AQP4-OAP disaggregation could work as a sensor, enabling tumor cells to evade normal apoptotic signaling (50) and acquire invasiveness potential. In particular, we show here that the role of the actin cytoskeleton in transducing the apoptotic signal might be dependent not only on AQP4 organization into OAPs, but also on AQP4 having a free C-terminus domain in which two Prolines seem to play a key role. This view is in line with the dramatic change in the actin cytoskeleton, reported upon cellular transformation, allowing metastatic properties such as increased cell migration and anchorage-independent growth.

We finally demonstrate that AQP4-OAP–transfected glioma cells display a higher content of F-actin, which appears to form a protein complex cosedimenting with AQP4-OAPs. Once again, this effect was found to be more prominent for U87 MG than for U251 MG cells, in line with the more dramatic changes in cell morphology and cytoskeleton observed in OAP-transfected U87 MG cells than in U251 MG. In healthy astrocytes, the relationship between AQP4 and the cell cytoskeleton has been previously discussed (8, 9) in terms of functional rather than physical interaction, which is important during cell adhesion, when astrocytes change their morphology going from a round shape to a flat fibroblast-like shape. It has also been shown that a higher content of F-actin is typical of astrocytes in their flat stable shape when movements are reduced to their base levels (8). Therefore, the stabilization of the cell cytoskeleton, with a higher content of F-actin, found here for AQP4-OAP–expressing glioma cells, is compatible with their very low migration potential being directed to apoptosis rather than invasiveness. Also in glioma cells, as for healthy astrocytes, negative results obtained in coimmunoprecipitation experiments between AQP4 and actin indicate a very labile interaction probably mediated by syntrophin or other unknown proteins.

In conclusion, given the correlation between OAP disaggregation and glioma invasiveness already reported (48) and based on the data here obtained, we can speculate that the aggregation state of AQP4 could be one of the keys in orienting glioma cells to perish through the activation of the apoptotic path, or to persist by potentiating their invasiveness potential. In this work, we gain insight into the complex role of AQP4 in tumor biology, showing a new perspective in which AQP4 role in glioma is not necessarily associated with edema formation but with the still mysterious role of AQP4 aggregation into OAPs and its link with the actin cytoskeleton.

Disclosure of Potential Conflicts of Interest

A.L. Vescovi is CEO CSO at Stemgen Spa and Hyperstem SA, and has an ownership interest (including stock, patents, etc.) in Hyperstem SA. No potential conflicts of interest were disclosed by the other authors.

Authors' Contributions

Conception and design: A. Frigeri, M. Svelto, G.P. Nicchia
Development of methodology: L. Simone, F. Pisani, M.G. Mola, M. De Bellis
Acquisition of data (provided animals, acquired and managed patients, provided facilities, etc.): G. Merla, L. Micale
Analysis and interpretation of data (e.g., statistical analysis, biostatistics, computational analysis): L. Simone, A. Frigeri, G.P. Nicchia
Writing, review, and/or revision of the manuscript: L. Simone, A. Frigeri, M. Svelto, G.P. Nicchia
Administrative, technical, or material support (i.e., reporting or organizing data, constructing databases): L. Simone, F. Pisani, M.G. Mola, M. De Bellis, A.L. Vescovi
Study supervision: G.P. Nicchia

Acknowledgments

This work was supported by a grant from the Italian Ministry of the University and Research (FIRB-Futuro in Ricerca RBFR12SJA8) to G.P. Nicchia. F. Pisani received a fellowship from Apulia Region (FIR—Future In Research, 5CU9HC5). The authors would like to thank Richard Lusardi for his assistance in revising the English of the article and Gaetano Devito for excellent technical assistance.

The costs of publication of this article were defrayed in part by the payment of page charges. This article must therefore be hereby marked *advertisement* in accordance with 18 U.S.C. Section 1734 solely to indicate this fact.

Received July 3, 2018; revised January 2, 2019; accepted March 11, 2019; published first March 15, 2019.

References

1. Nagelhus EA, Ottersen OP. Physiological roles of aquaporin-4 in brain. Physiol Rev 2013;93:1543–62.
2. Smith AJ, Verkman AS. Superresolution imaging of aquaporin-4 cluster size in antibody-stained paraffin brain sections. Biophys J 2015;109:2511–22.
3. Silberstein C, Bouley R, Huang Y, Fang P, Pastor-Soler N, Brown D, et al. Membrane organization and function of M1 and M23 isoforms of aquaporin-4 in epithelial cells. Am J Physiol Renal Physiol 2004;287:F501–11.
4. Smith AJ, Jin BJ, Ratelade J, Verkman AS. Aggregation state determines the localization and function of M1- and M23-aquaporin-4 in astrocytes. J Cell Biol 2014;204:559–73.
5. Hiroaki Y, Tani K, Kamegawa A, Gyobu N, Nishikawa K, Suzuki H, et al. Implications of the aquaporin-4 structure on array formation and cell adhesion. J Mol Biol 2006;355:628–39.
6. Neely JD, Amiry-Moghaddam M, Ottersen OP, Froehner SC, Agre P, Adams ME. Syntrophin-dependent expression and localization of Aquaporin-4 water channel protein. Proc Natl Acad Sci U S A 2001;98:14108–13.
7. Nicchia GP, Rossi A, Nudel U, Svelto M, Frigeri A. Dystrophin-dependent and -independent AQP4 pools are expressed in the mouse brain. Glia 2008;56:869–76.
8. Nicchia GP, Rossi A, Mola MG, Procino G, Frigeri A, Svelto M. Actin cytoskeleton remodeling governs aquaporin-4 localization in astrocytes. Glia 2008;56:1755–66.
9. Nicchia GP, Srinivas M, Li W, Brosnan CF, Frigeri A, Spray DC. New possible roles for aquaporin-4 in astrocytes: cell cytoskeleton and functional relationship with connexin43. FASEB J 2005;19:1674–6.
10. Papadopoulos MC, Saadoun S. Key roles of aquaporins in tumor biology. Biochim Biophys Acta 2015;1848:2576–83.
11. Maugeri R, Schiera G, Di Liegro CM, Fricano A, Iacopino DG, Di Liegro I. Aquaporins and brain tumors. Int J Mol Sci 2016;17.
12. Yang WY, Tan ZF, Dong DW, Ding Y, Meng H, Zhao Y, et al. Association of aquaporin1 with tumor migration, invasion and vasculogenic mimicry in glioblastoma multiforme. Mol Med Rep 2018;17:3206–11.

Published OnlineFirst March 15, 2019; DOI: 10.1158/0008-5472.CAN-18-2015

13. Saadoun S, Papadopoulos MC, Hara-Chikuma M, Verkman AS. Impairment of angiogenesis and cell migration by targeted aquaporin-1 gene disruption. Nature 2005;434:786–92.
14. Nicchia GP, Stigliano C, Sparaneo A, Rossi A, Frigeri A, Svelto M. Inhibition of aquaporin-1 dependent angiogenesis impairs tumour growth in a mouse model of melanoma. J Mol Med (Berl) 2013;91:613–23.
15. Lan YL, Wang X, Lou JC, Ma XC, Zhang B. The potential roles of aquaporin 4 in malignant gliomas. Oncotarget 2017;8:32345–55.
16. Wolburg H, Noell S, Fallier-Becker P, Mack AF, Wolburg-Buchholz K. The disturbed blood-brain barrier in human glioblastoma. Mol Aspects Med 2012;33:579–89.
17. Noell S, Wolburg-Buchholz K, Mack AF, Ritz R, Tatagiba M, Beschorner R, et al. Dynamics of expression patterns of AQP4, dystroglycan, agrin and matrix metalloproteinases in human glioblastoma. Cell Tissue Res 2012; 347:429–41.
18. Fallier-Becker P, Nieser M, Wenzel U, Ritz R, Noell S. Is upregulation of aquaporin 4-M1 isoform responsible for the loss of typical orthogonal arrays of particles in astrocytomas? Int J Mol Sci 2016;17.
19. Furman CS, Gorelick-Feldman DA, Davidson KG, Yasumura T, Neely JD, Agre P, et al. Aquaporin-4 square array assembly: opposing actions of M1 and M23 isoforms. Proc Natl Acad Sci U S A 2003;100:13609–14.
20. Motaln H, Koren A, Gruden K, Ramsak Z, Schichor C, Lah TT. Heterogeneous glioblastoma cell cross-talk promotes phenotype alterations and enhanced drug resistance. Oncotarget 2015;6:40998–1017.
21. Li H, Lei B, Xiang W, Wang H, Feng W, Liu Y, et al. Differences in protein expression between the U251 and U87 cell lines. Turk Neurosurg 2017;27: 894–903.
22. Nicchia GP, Pisani F, Simone L, Cibelli A, Mola MG, Dal Monte M, et al. Glio-vascular modifications caused by Aquaporin-4 deletion in the mouse retina. Exp Eye Res 2016;146:259–68.
23. Mola MG, Sparaneo A, Gargano CD, Spray DC, Svelto M, Frigeri A, et al. The speed of swelling kinetics modulates cell volume regulation and calcium signaling in astrocytes: a different point of view on the role of aquaporins. Glia 2016;64:139–54.
24. Ponten J, Macintyre EH. Long term culture of normal and neoplastic human glia. Acta Pathol Microbiol Scand 1968;74:465–86.
25. Benda P, Lightbody J, Sato G, Levine L, Sweet W. Differentiated rat glial cell strain in tissue culture. Science 1968;161:370–1.
26. Radany EH, Brenner M, Besnard F, Bigornia V, Bishop JM, Deschepper CF. Directed establishment of rat brain cell lines with the phenotypic characteristics of type 1 astrocytes. Proc Natl Acad Sci U S A 1992;89: 6467–71.
27. Fidler IJ. Selection of successive tumour lines for metastasis. Nat New Biol 1973;242:148–9.
28. Macville M, Schrock E, Padilla-Nash H, Keck C, Ghadimi BM, Zimonjic D, et al. Comprehensive and definitive molecular cytogenetic characterization of HeLa cells by spectral karyotyping. Cancer Res 1999;59:141–50.
29. Westermark B, Ponten J, Hugosson R. Determinants for the establishment of permanent tissue culture lines from human gliomas. Acta Pathol Microbiol Scand A 1973;81:791–805.
30. Rossi A, Pisani F, Nicchia GP, Svelto M, Frigeri A. Evidences for a leaky scanning mechanism for the synthesis of the shorter M23 protein isoform of aquaporin-4: implication in orthogonal array formation and neuromyelitis optica antibody interaction. J Biol Chem 2010;285:4562–9.
31. Korkotian E, Schwarz A, Pelled D, Schwarzmann G, Segal M, Futerman AH. Elevation of intracellular glucosylceramide levels results in an increase in endoplasmic reticulum density and in functional calcium stores in cultured neurons. J Biol Chem 1999;274:21673–8.
32. Bunnell TM, Ervasti JM. Delayed embryonic development and impaired cell growth and survival in Actg1 null mice. Cytoskeleton (Hoboken) 2010; 67:564–72.
33. Ho JD, Yeh R, Sandstrom A, Chorny I, Harries WE, Robbins RA, et al. Crystal structure of human aquaporin 4 at 1.8 A and its mechanism of conductance. Proc Natl Acad Sci U S A 2009;106:7437–42.
34. Albini A, Benelli R. The chemoinvasion assay: a method to assess tumor and endothelial cell invasion and its modulation. Nat Protoc 2007;2: 504–11.
35. Frankowski H, Gu YH, Heo JH, Milner R, Del Zoppo GJ. Use of gel zymography to examine matrix metalloproteinase (gelatinase) expression in brain tissue or in primary glial cultures. Methods Mol Biol 2012;814: 221–33.
36. Parhi P, Suklabaidya S, Kumar Sahoo S. Enhanced anti-metastatic and anti-tumorigenic efficacy of Berbamine loaded lipid nanoparticles in vivo. Sci Rep 2017;7:5806.
37. Xue Q, Cao L, Chen XY, Zhao J, Gao L, Li SZ, et al. High expression of MMP9 in glioma affects cell proliferation and is associated with patient survival rates. Oncol Lett 2017;13:1325–30.
38. Pisani F, Mastrototaro M, Rossi A, Nicchia GP, Tortorella C, Ruggieri M, et al. Identification of two major conformational aquaporin-4 epitopes for neuromyelitis optica autoantibody binding. J Biol Chem 2011;286: 9216–24.
39. Guruprasad K, Rajkumar S. Beta-and gamma-turns in proteins revisited: a new set of amino acid turn-type dependent positional preferences and potentials. J Biosci 2000;25:143–56.
40. Noell S, Ritz R, Wolburg-Buchholz K, Wolburg H, Fallier-Becker P. An allograft glioma model reveals the dependence of aquaporin-4 expression on the brain microenvironment. PLoS One 2012;7:e36555.
41. Auguste KI, Jin S, Uchida K, Yan D, Manley GT, Papadopoulos MC, et al. Greatly impaired migration of implanted aquaporin-4-deficient astroglial cells in mouse brain toward a site of injury. FASEB J 2007;21:108–16.
42. Saadoun S, Papadopoulos MC, Watanabe H, Yan D, Manley GT, Verkman AS. Involvement of aquaporin-4 in astroglial cell migration and glial scar formation. J Cell Sci 2005;118:5691–8.
43. McCoy E, Sontheimer H. Expression and function of water channels (aquaporins) in migrating malignant astrocytes. Glia 2007;55:1034–43.
44. Simone L, Gargano CD, Pisani F, Cibelli A, Mola MG, Frigeri A, et al. Aquaporin-1 inhibition reduces metastatic formation in a mouse model of melanoma. J Cell Mol Med 2018;22:904–12.
45. Arif T, Vasilkovsky L, Refaely Y, Konson A, Shoshan-Barmatz V. Silencing VDAC1 expression by siRNA inhibits cancer cell proliferation and tumor growth in vivo. Mol Ther Nucleic Acids 2014;3:e159.
46. Rossi A, Baumgart F, van Hoek AN, Verkman AS. Post-Golgi supramolecular assembly of aquaporin-4 in orthogonal arrays. Traffic 2012;13: 43–53.
47. Jablonski EM, Webb AN, McConnell NA, Riley MC, Hughes FM Jr. Plasma membrane aquaporin activity can affect the rate of apoptosis but is inhibited after apoptotic volume decrease. Am J Physiol Cell Physiol 2004;286:C975–85.
48. Thompson EG, Sontheimer H. A role for ion channels in perivascular glioma invasion. Eur Biophys J 2016;45:635–48.
49. Hoddevik EH, Khan FH, Rahmani S, Ottersen OP, Boldt HB, Amiry-Moghaddam M. Factors determining the density of AQP4 water channel molecules at the brain-blood interface. Brain Struct Funct 2017;222: 1753–66.
50. Desouza M, Gunning PW, Stehn JR. The actin cytoskeleton as a sensor and mediator of apoptosis. Bioarchitecture 2012;2:75–87.

Published OnlineFirst March 15, 2019; DOI: 10.1158/0008-5472.CAN-18-2015

Cancer Research
The Journal of Cancer Research (1916–1930) | The American Journal of Cancer (1931–1940)

AACR American Association for Cancer Research

AQP4 Aggregation State Is a Determinant for Glioma Cell Fate

Laura Simone, Francesco Pisani, Maria G. Mola, et al.

Cancer Res 2019;79:2182-2194. Published OnlineFirst March 15, 2019.